Evaluation of Dual–Time-Point ^{18}F-FDG PET for Staging in Patients with Lung Cancer

Daisuke Uesaka[1], Yoshiki Demura[1], Takeshi Ishizaki[1], Shingo Ameshima[1], Isamu Miyamori[2], Masato Sasaki[3], Yasuhisa Fujibayashi[4], and Hidehiko Okazawa[4]

[1]Department of Respiratory Medicine, University of Fukui, Fukui, Japan; [2]Third Department of Internal Medicine, University of Fukui, Fukui, Japan; [3]Department of Thoracic Surgery, University of Fukui, Fukui, Japan; and [4]Biochemical Imaging Reserch Center, University of Fukui, Fukui, Japan

^{18}F-FDG PET is increasingly used for lung cancer; however, some insufficient results have been reported. The purpose of this study was to evaluate the efficacy of dual–time-point ^{18}F-FDG PET for staging lung cancer and for differentiating metastatic from nonmetastatic lung cancer lesions. **Methods:** One hundred fifty-five lung cancer patients with known or suspected mediastinal and hilar lymph node involvement or distant metastases underwent whole-body ^{18}F-FDG PET at 2 time points: scan 1 at 60 min (early imaging) and scan 2 at 180 min (delayed imaging) after ^{18}F-FDG injection. ^{18}F-FDG PET findings of nodal and distant metastases were evaluated using conventional imaging, clinical follow-up findings, and the results of autopsy or biopsy. **Results:** A total of 580 lesions (155 primary lesions, 315 metastatic lesions, and 110 nonmetastatic lesions) were used for analysis. A closer correlation between the primary lesions and metastases was observed for the retention index (RI) standardized uptake value (SUV) than for early and delayed SUV. There was no relationship between the RI SUV results of primary lesions and those of nonmetastatic lesions. The RI SUV of metastatic lesions was approximately 0.5–2 times the RI SUV of primary tumors. We found that the accuracy of ^{18}F-FDG PET was improved when RI SUV was used for detecting lymph node and distant metastases, because of the significant improvement in specificity relative to early and delayed SUV. **Conclusion:** RI SUV raised the accuracy for diagnosis of metastases and was superior to early and delayed imaging in terms of differentiating malignancy from nonmetastatic uptake.

Key Words: lung cancer; ^{18}F-FDG PET; staging; dual–time-point imaging; delayed PET

J Nucl Med 2008; 49:1606–1612
DOI: 10.2967/jnumed.108.051250

Lung cancer is the leading cause of cancer-related death in Japan. Precise diagnosis of the patient's stage of lung cancer is important for determining prognosis and treatment options. ^{18}F-FDG PET, which is increasingly used for diagnosing, staging, and determining the type of lung cancer (*1–3*), can obtain images that reflect physiologic and biochemical function and is therefore useful in the differential diagnosis of benign and malignant lesions (*4–6*). However, there are numerous causes of ^{18}F-FDG uptake in benign processes (*7,8*), and this nonspecific uptake is a potential source of false-positive results in ^{18}F-FDG PET (*3,9,10*) even when PET/CT is also used (*11–13*). This major problem must be resolved in ^{18}F-FDG PET examinations. Recent studies show poor accuracy of ^{18}F-FDG PET in nodal staging (*14–16*). If we could precisely diagnose the reason for ^{18}F-FDG accumulation, additional examinations would not be necessary.

We recently reported that the retention index (RI) standardized uptake value (SUVs) calculated from delayed ^{18}F-FDG PET provide a significantly more accurate diagnosis in lung cancer than does early ^{18}F-FDG PET and chest CT and that a close correlation exists between the RI SUV results for the primary lesion and lymph node metastases (*4*); however, there are far fewer ^{18}F-FDG PET studies, especially for dual–time-point ^{18}F-FDG PET, regarding the staging of distant organ sites than there are regarding the staging of mediastinal lymph nodes (*1–3*).

Therefore, we hypothesized that dual–time-point ^{18}F-FDG PET may improve the accuracy of staging in patients with lung cancer. We tested this hypothesis in a consecutive series of lung cancer patients undergoing staging.

MATERIALS AND METHODS

Patients

We prospectively studied patients with lung cancer and with known or suspected mediastinal and hilar lymph node involvement or distal metastases diagnosed on the basis of radiologic findings (e.g., chest CT). Lung cancer was staged according to final clinical and radiologic follow-up and pathologic findings. The study was approved by the Institutional Review Board of our hospital, and written informed consent was obtained from all patients participating.

Patients who had hyperglycemia (blood glucose levels $>$ 126 mg/dL at the time of ^{18}F-FDG injection) before ^{18}F-FDG PET examination were excluded from the study. The ^{18}F-FDG PET findings for all primary lesions and all nodal involvement were

Received Jan. 29, 2008; revision accepted Apr. 3, 2008.
For correspondence or reprints contact: Yoshiki Demura, Department of Respiratory Medicine, University of Fukui, 23-3 Matsuokashimoaizuki, Eiheiji-cho, Yoshida-gun Fukui 910-1193 Japan.
E-mail: DEM2180@aol.com

TABLE 1
Patient Characteristics

Characteristic	Value
Total patients (*n*)	155
M/F (*n*)	115/40
Mean age (y)	69 ± 9
Age range (y)	45–89
Histopathologic type (*n*)	
Adenocarcinoma	83
Squamous cell carcinoma	54
Small cell carcinoma	13
Large cell carcinoma	3
Atypical carcinoid	1
Unclassified	1
Stage (*n*)	
IA	30
IB	15
IIA	2
IIB	4
IIIA	27
IIIB	10
IV	67

compared within 4 wk with the histopathologic diagnosis. The histopathologic diagnoses of all mediastinal and hilar lymph nodes were confirmed by surgical resection or videomediastinoscopy. All supraclavicular and cervical lymph node metastases were determined by surgical resection or needle biopsy. PET findings of distant metastases, except for brain metastases, were further evaluated by the findings of radiologic examinations performed within 2 wk of PET (CT of the chest and abdomen, ultrasonography of the abdomen, MRI of bone and soft tissue, and a ^{99m}Tc bone scan), the results of autopsy or biopsy, and the clinical follow-up findings. The clinical follow-up period was at least 9 mo. Patients were examined regularly every month, during which history, physical examination, and radiologic findings were collected, as well as the findings of additional investigations as necessary. All patients underwent ^{18}F-FDG PET before biopsy and treatment of lung cancer.

^{18}F-FDG PET

We used a whole-body tomography scanner (ADVANCE; GE Healthcare), which permits simultaneous acquisition of 35 image slices in a 2-dimensional acquisition mode with interslice spacing of 4.25 mm. Performance tests showed the intrinsic resolution of the scanner to be 4.0–5.3 mm in the axial direction and 4.6–5.7 mm in the transaxial direction. All patients fasted overnight (for at least 12 h) before radiotracer administration. Approximately 185–370 MBq of ^{18}F-FDG were administered intravenously. Sixty minutes (the early scan) and 3 h (the delayed scan) after tracer injection, the patient was positioned supine in the PET scanner and a 16-min emission scan was performed, with 3-min scans at the thoracic region (2 bed positions) and 2-min scans in each remaining region (5 bed positions) to completely cover the head to inguinal areas. Postinjection transmission scans were obtained after the emission scans using a ^{68}Ge/^{68}Ga rod source for attenuation correction. The PET data were reconstructed by the iterative method, with selection of 14 subsets and 2 iterations. In each emission scan, the patient's body was carefully positioned with guidance from a laser beam to prevent misregistration.

^{18}F-FDG accumulations were considered positive when focal uptake was more intense than the mediastinal blood-pool activity in the early scan or delayed scan. PET images were interpreted independently and prospectively by experienced radiologists and nuclear medicine physicians, without knowledge of histopathologic or other radiologic data. Semiquantitative analysis of the ^{18}F-FDG uptake was based on region-of-interest analysis that produced mean SUVs (tumor activity concentration/injected dose/body weight), as described previously (*4*). The RI SUV was calculated from the results of 1 h (early scan) and 3 h (delayed scan) imaging according to the following equation: RI SUV (%) = (SUV [delayed scan] – SUV [early scan]) × 100/SUV (early scan).

CT

CT scans were obtained using a helical CT system (HiSpeed Advantage RP; GE Healthcare) or a 16-detector-row CT system (Sensation 16; Siemens). Contiguous 5- to 10-mm-thick sections were obtained at 5- to 10-mm intervals from the lung apices to the pelvis before and during intravenous bolus injection of contrast material at 2 mL/s by power injector. Transaxial images were

TABLE 2
Characteristics of Malignant Lesions and Methods of Diagnosis

Malignant lesion	Number of lesions	Surgery	Biopsy	Autopsy	Clinical follow-up
Primary lesion	155	76	77	2	
Mediastinal lymph node	85	24	59	2	
Hilar lymph node	15	15			
Supraclavicular lymph node	6		6		
Cervical lymph node	35		35		
Intraperitoneal lymph node	8			1	7
Bone	76		4	6	66
Liver	26		1	3	22
Pleura	24		5	7	12
Lung	23	3	4	4	12
Adrenal grand	6	1	1	1	3
Kidney	5			4	1
Peritoneum	3				3
Muscle, skin	2		2		
Invasion of atrium	1				1
Total	470	119	194	30	127

TABLE 3
Characteristics and Methods of Diagnosis for Nonmetastatic Uptake

Nonmetastatic uptake	Number of lesions	Surgery	Biopsy	Clinical follow-up
Lymph node (anthracosis)	20	20		
Lymph node (follicular hyperplasia)	9	9		
Lymph node (anthracosis and follicular hyperplasia)	3	3		
Lymph node (granulomatous inflammation)	12	12		
Pneumonia	8	5		3
Arthritis	4			4
Urinary tract, hydronephrosis	4			4
Malignancy of another organ (thyroid, larynx)	6	3	3	
Parotid tumor (Warthin tumor)	3	3		
Incidental colonic ^{18}F-FDG uptake	7			7
Inflammatory disease of abdomen (e.g., gastric ulcer, diverticulitis, or cholecystitis)	12	1	11	
Inflammatory disease of head and neck (e.g., sinusitis, parotiditis, or chronic thyroiditis)	21		4	17
Extravasation of ^{18}F-FDG	1			1
Total	110	56	18	36

obtained for all patients. Mediastinal and hilar lymph nodes were assessed if they were larger than 7 mm in short-axis diameter on transaxial chest CT images.

Statistical Analysis

The results of ^{18}F-FDG are expressed as mean ± SD. In early and delayed imaging and in RI SUV, Pearson correlation coefficient analysis and simple regression were used to assess the relationship between the primary tumor and metastatic or nonmetastatic lesions. We examined the difference between each correlation coefficient using the z-transformation. We examined the 95% prediction interval of RI SUV of metastatic lesions using simple regression analysis. We calculated linear approximations for the upper and lower bounds of the 95% prediction interval and set the threshold for the metastatic lesion using RI SUV. The sensitivity, specificity, and diagnostic accuracy of early imaging, delayed imaging, and RI SUV were determined. The 95% confidence interval (95% CI) is given for each parameter. The diagnostic accuracy of each method was compared using the McNemar test. For all analyses, P values less than 0.05 were considered statistically significant.

RESULTS

Subject Demography and Clinical Characteristics

We evaluated 160 consecutive patients between April 2000 and March 2007. Five patients were subsequently excluded because of atypical mycobacteriosis, pneumonia, and lymphoma. Thus, 155 patients (115 men and 40 women; age range, 45–89 y; mean age, 69 ± 9 y) were included in the present study. The characteristics of the 155 evaluated patients are shown in Table 1.

In these patients, we evaluated 580 lesions considered to be positive for uptake on early ^{18}F-FDG PET: 470 sites of uptake were malignant lesions, whereas 110 sites were nonmetastatic. Table 2 shows the details of the 470 malignant lesions; Table 3 shows the causes of the 110 sites of nonmetastatic uptake. The diagnosis method is noted on the right-hand side of these tables.

Correlation Between SUV Levels of Primary Tumor and Metastatic Lesion

Figure 1 shows the strong correlation between the RI SUV of the primary lesion and the metastatic lesion (r = 0.783). The r value of RI SUV was significantly higher than that of early and delayed SUV ($P < 0.0001$). Using the results of the 95% prediction interval of the simple regression analysis for RI SUV of metastatic lesions, the upper linear approximation becomes $y = 1.534x + 6.417$ and the lower linear approximation becomes $y = 0.426x + 0.886$ (straight pink line in Fig. 1). To simplify the results of the

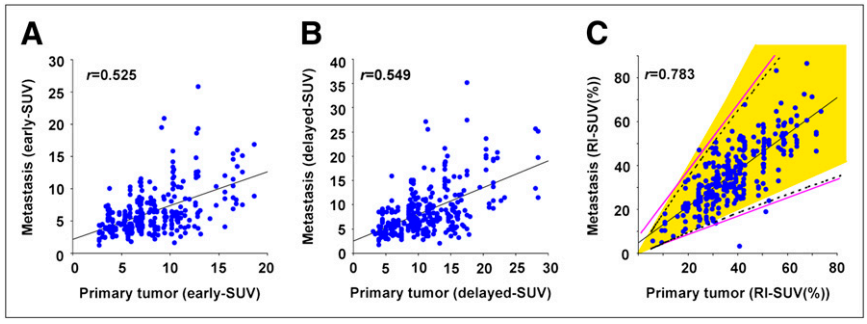

FIGURE 1. Correlation between SUV levels of all metastases and primary tumors in PET of lung cancer patients: early imaging ($y = 0.523x + 2.123$; $r = 0.525$) (A); delayed imaging ($y = 0.551x + 2.542$; $r = 0.549$) (B); and RI SUV ($y = 0.829x + 4.667$; $r = 0.783$) (C). Using RI SUV results of 95% prediction interval (broken line), upper linear approximation becomes $y = 1.534x + 6.417$ and lower linear approximation becomes $y = 0.426x + 0.886$ (straight pink lines). We indicated yellow area (0.5–2 times RI SUV of primary tumors) for deciding on metastatic lesions.

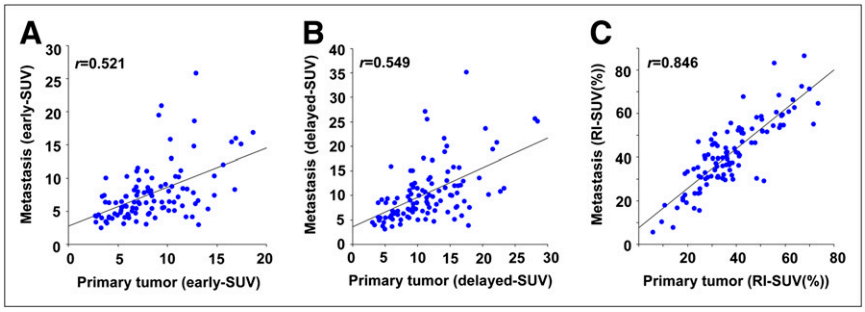

FIGURE 2. Correlation between highest SUV levels of all metastases and primary tumors in PET of lung cancer patients: early imaging ($y = 0.59x + 2.751$; $r = 0.521$) (A); delayed imaging ($y = 0.605x + 3.569$; $r = 0.549$) (B); and RI SUV ($y = 0.904x + 7.619$; $r = 0.846$) (C).

95% prediction interval of the simple regression analysis for RI SUV of metastatic lesions, we chose a value of approximately 2 for the ideal upper cutoff and a value of approximately 0.5 for the ideal lower cutoff (yellow area in Fig. 1) for RI SUV of metastatic lesion/RI SUV of primary lesion. Figure 2 shows the strong correlation between the highest RI SUV of the primary lesion and the metastatic lesion ($r = 0.846$). The r value of the highest RI SUV was significantly higher than that of the highest early and delayed SUV ($P < 0.0001$). We examined cases that initially were positive for ^{18}F-FDG uptake but were later identified as nonmetastatic findings. There was no relationship between the RI SUV of the primary uptake and the RI SUV of the nonmetastatic uptake (data not shown).

RI SUV in Distinguishing Metastatic Lesions from Nonmetastatic Lesions

Figures 3A and 3B compare the SUV levels of all sites of remote uptake and all primary tumors on ^{18}F-FDG PET images of lung cancer patients. Uptake in metastases was almost indistinguishable from that in nonmetastatic lesions on early and delayed imaging. When positive ^{18}F-FDG PET findings are defined as linear approximations of the upper and lower bounds of the 95% prediction interval of RI SUV, the results of RI SUV based on a lesion-by-lesion analysis demonstrate a sensitivity of 98% (95% CI, 96%−99%), specificity of 94% (95% CI, 89%−97%), and accuracy of 97% (95% CI, 95%−98%). When positive ^{18}F-FDG PET findings are defined as the yellow area of RI SUV ratio (remote site/primary site) shown in Figure 3C, the RI SUV results demonstrate a sensitivity of 98% (95% CI, 96%−100%), specificity of 93% (95% CI, 86%−97%), and accuracy of 97% (95% CI, 95%−98%). These 2 criteria had few differences in diagnostic accuracy; therefore, we defined the diagnosing criterion on ^{18}F-FDG PET as the yellow region.

Comparison of Single- and Dual–Time-Point ^{18}F-FDG PET Results for N and M Staging

A comparison of single- and dual–time-point ^{18}F-FDG PET on a patient-by-patient basis is shown in Table 4 for the evaluation of nodal staging and in Table 5 for the evaluation of distant metastasis staging. The accuracy of ^{18}F-FDG PET was improved when RI SUV was used in detecting lymph node metastases and distant metastases because of the significant improvement in specificity relative to early and delayed SUV ($P < 0.001$, McNemar test). Table 6 shows the effect of the RI SUV method for correcting misdiagnosis in over- or understaged lung cancer. In no cases were metastatic lesions negative on early imaging but positive on delayed imaging. Figure 4 shows a representative case of adenocarcinoma and mediastinal lymph node metastasis. The RI SUV of the primary tumor was nearly consistent with that of the lymph node metastasis. Figure 5 shows the RI SUV of a representative patient with lung cancer and a sarcoid reaction in the mediastinal lymph nodes. We were unable to visually distinguish a sarcoid reaction from lymph node metastases on early and delayed imaging. Using our RI SUV criteria, no evidence of lymph node metastasis was seen.

False-Positive and False-Negative Results in RI SUV

Eight sites of uptake were false-positive RI SUV findings: 6 inflammatory lesions, 1 cancerous lesion, and 1 benign tumor. Five lesions had false-negative findings: 3 bone metastases and 2 liver metastases.

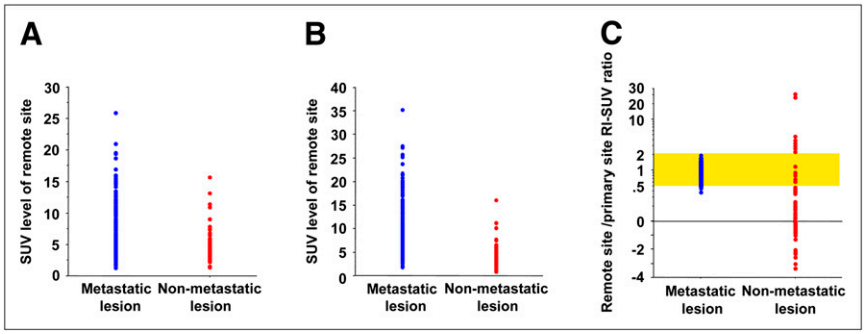

FIGURE 3. Comparison of SUV level (early and delayed) and RI SUV ratio of primary lesion and remote site (blue = metastatic uptake; red = nonmetastatic uptake): early imaging (A), delayed imaging (B), and RI SUV (C). In cases in which PET-positive findings are defined as yellow area (0.5–2 times RI SUV of primary tumors), uptakes of metastatic and nonmetastatic lesions are distinguishable.

TABLE 4
Comparison of Single- and Dual–Time-Point ^{18}F-FDG PET Results for Staging of Nodal Metastasis Based on Patient-by-Patient Analysis (Surgical Cases and Definitive Pathologic N3 cases)

Parameter	Number of patients				Sensitivity		Specificity		Accuracy	
	N0 (TN)	N1	N2	N3	%	95% CI (%)	%	95% CI (%)	%	95% CI (%)
Early imaging	29/45	4/6	21/21	2/2	93	77–99	64*	49–78	76*	64–85
Delayed imaging	33/45	5/6	21/21	2/2	97	82–100	73*	58–85	82*	72–90
RI SUV	44/45	6/6	21/21	2/2	100		98	88–99	99	93–100

*$P < 0.001$ vs. RI SUV using McNemar test.

DISCUSSION

To our knowledge, this is the first report to describe the dual–time-point ^{18}F-FDG PET technique as a means of providing diagnostic criteria for lung cancer metastases. In this study, we demonstrated a close correlation between the RI SUV of the primary and metastatic lesions.

In most ^{18}F-FDG PET studies, imaging is performed 50–60 min after ^{18}F-FDG injection (*17*); however, the uptake of ^{18}F-FDG in malignancies is expected to increase over 1.5–5 h (*18*). In theory, images obtained 2–3 h after ^{18}F-FDG injection should show improved contrast between tumor and normal tissues or benign processes, because uptake is increased in the tumor and decreased in the normal background (*19,20*). Several recent studies have described the advantages of delayed imaging with ^{18}F-FDG, particularly in the diagnosis of cervical and breast cancer (*21,22*); however, it is reported that in differentiating malignant from benign lesions, the accuracy of RI SUV in dual–time-point ^{18}F-FDG PET is higher than that of delayed ^{18}F-FDG PET alone (*4,23,24*). The results of our study suggest that dual–time-point ^{18}F-FDG PET is appropriate for the staging of lung cancer, and we therefore recommend the RI SUV of dual–time-point ^{18}F-FDG PET as a highly useful diagnostic tool in diagnosing lung cancer.

It is well recognized that current nodal staging procedures in patients with lung cancer have a limitation for accurate diagnosis, even when ^{18}F-FDG PET is used. Previous reports demonstrate the advantages and limitations of ^{18}F-FDG PET in nodal staging (*10–16*). The major problem with this modality is inadequate specificity in mediastinal staging, although the modality is more efficient than CT. ^{18}F-FDG accumulation on PET or PET/CT had a high sensitivity for malignancy but was also seen in many kinds of inflammatory lymph node swelling, thus reducing diagnostic specificity (*11,25,26*). In the present study, the specificity of nodal staging on early imaging was only 64% in patients with mediastinal and hilar lymphadenopathy. In surgical cases, we assessed the pathologic findings for mediastinal and hilar lymph nodes that had false-positive ^{18}F-FDG accumulation on early imaging. Anthracosis, follicular hyperplasia, and granulomatous inflammation were most commonly recognized in these false-positive lymph nodes when compared with ^{18}F-FDG–negative lymph nodes. We previously reported active granulomatous disease to have a mean RI SUV of 41.2% (*4*).

^{18}F-FDG PET sometimes reveals unexpected distant metastases that were negative or equivocal findings on conventional staging (*27,28*); however, a disadvantage of single-time-point ^{18}F-FDG PET is the normal physiologic accumulation of ^{18}F-FDG in the liver, bowel, kidney, urinary tract, and muscles and in benign processes such as inflammation, making visual evaluation of metastases at these sites difficult. Furthermore, ^{18}F-FDG PET studies sometimes detect sites of distant metastasis that are false-positive (*28,29*). Our RI SUV criteria showed a diagnostic accuracy of 99% for distant metastasis (M stage) because they enable malignant uptake to be differentiated from the

TABLE 5
Comparison of Single- and Dual–Time-Point ^{18}F-FDG PET Results for Staging of Distant Metastasis Based on Patient-by-Patient Analysis

Parameter	Number of patients				Sensitivity		Specificity		Accuracy	
	TP	TN	FP	FN	%	95% CI (%)	%	95% CI (%)	%	95% CI (%)
Early imaging	67	52	36	0	100		59*	48–70	77*	69–83
Delayed imaging	67	58	30	0	100		66*	55–76	81*	74–87
RI SUV	67	86	2	0	100		98	92–100	99	95–100

*$P < 0.001$ vs. RI SUV using McNemar test.
TP = true-positive; TN = true-negative; FP = false-positive; FN = false-negative.

TABLE 6
Effect of RI SUV Method for Restaging of Misdiagnosed Lung Cancer Patients

Stage	No. of patients	Number of patients overstaged (false-positive)			Number of patients understaged (false-negative)		
		Early imaging	Delayed imaging	RI SUV	Early imaging	Delayed imaging	RI SUV
N0	45	16	12	1	—	—	—
N1	6	2	1	0	0	0	0
N2	21	0	0	0	0	0	0
N3	2	0	0	0	0	0	0
N staging overall	74	18 (24%)	13 (18%)	1 (1%)	0	0	0
M0	88	36	30	2	—	—	—
M1	67	—		—	0	0	0
M staging overall	155	36 (23%)	30 (19%)	2 (1%)	0	0	0

normal physiologic background level, benign processes, and even inflammatory diseases.

In the present study, the RI SUV had a stronger correlation between primary lesions and metastases than did the SUV level of early imaging and delayed imaging. The primary lesion and metastasis could have the same malignant cell characteristics. The SUV level of the tumor can be influenced by tumor size, tumor cell density, and blood flow (*30*); however, the RI of the SUV level can reflect glucose phosphorylation, which may in turn be related to cell proliferation in the absence of such an influence (*31,32*). If the accumulation or washout of ^{18}F-FDG in remote sites differs from that in the primary site on delayed imaging, the remote sites should have a different pathologic process from the primary lesion. Therefore, the RI SUV criteria are more useful in the diagnosis of nodal and distant metastases. We propose that dual–time-point PET is useful for cases of hilar or mediastinal lymph node swelling and cases doubtful for metastasis because of abnormal uptake on early images.

According to our criteria, there were only 8 sites of false-positive uptake for RI SUV: pneumonia requiring antibiotic therapy, pneumonia-induced follicular hyperplasia in a hilar

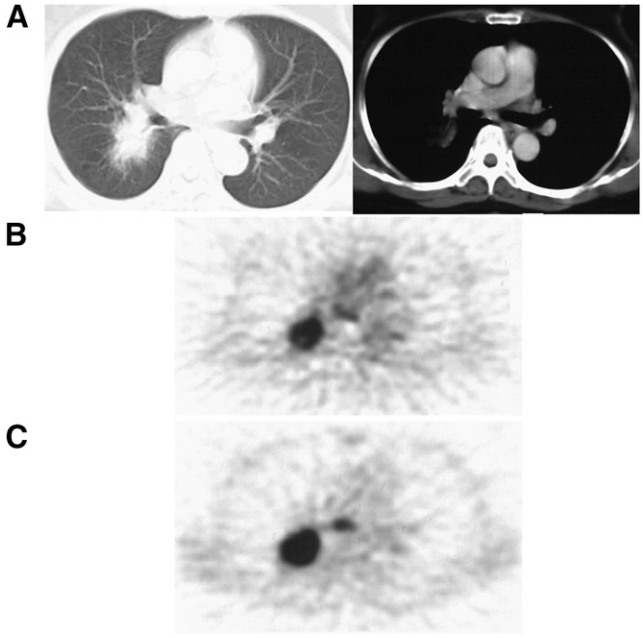

FIGURE 4. Representative case of adenocarcinoma and mediastinal lymph node metastasis (lymph node 7) in subcarinal area: chest CT (A), early imaging (B), and delayed imaging (C). CT images show nodule in right lung with no significant mediastinal lymph node swelling. Early imaging shows strong accumulation in nodule and faint accumulation in lymph node 7. PET shows increased uptake in lung nodule (early SUV = 6.85, delayed SUV = 10.01, RI SUV = 46.1%) and uptake in lymph node 7 (early SUV = 3.49, delayed SUV = 5.08, RI SUV = 45.6%).

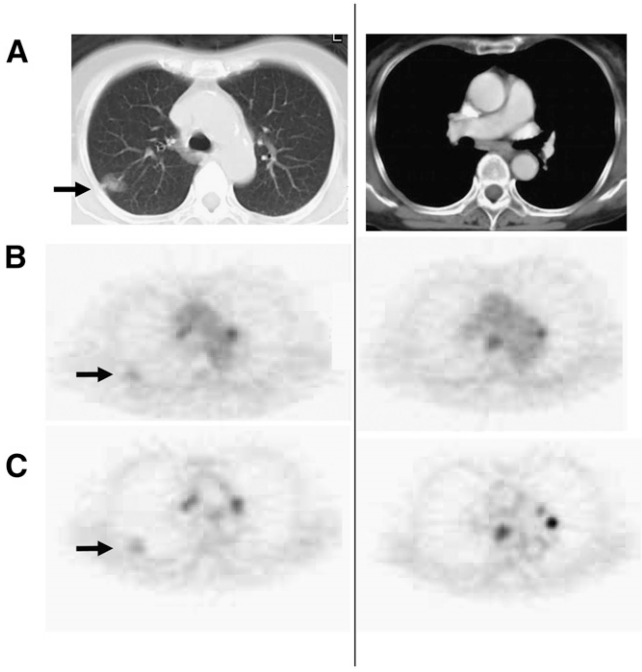

FIGURE 5. Representative case of adenocarcinoma and sarcoid reaction of mediastinal lymph node swelling: chest CT (A), early imaging (B), and delayed imaging (C). PET showed ^{18}F-FDG uptake in primary tumor (early SUV = 1.81, delayed SUV = 2.02) (arrows) and focal uptake in mediastinal lymph nodes (lymph node 3: early SUV = 2.91, delayed SUV = 4.2; lymph node 7: early SUV = 3.89, delayed SUV = 5.086). RI SUV in primary tumor was 11.6%; however, RI SUVs in these lymph nodes were much higher (30.8%−44.3%). These nodal uptakes were confirmed at surgery as sarcoid reaction.

lymph node, an abscess in the small intestine that required surgery, and laryngeal cancer, among others. We considered the necessity of infection control before PET examination to reduce false-positive uptake. False-negative findings in bone have been reported in cases of osteoblastic lesions (*33*). In the false-negative cases of the present study in patients with bone metastasis, the histopathologic finding was osteolytic lesions, which suggests a low number of tumor cells and a high degree of fibrosis compared with the true-positive cases.

CONCLUSION

Our study indicates criteria for the staging of lung cancer and suggests new examination methods for the noninvasive evaluation of lung cancer using PET. According to our criteria, an improvement in the diagnostic specificity of PET examinations implies that additional examinations can be eliminated, thereby saving medical costs. On the basis of our preliminary data, we intend to perform additional examinations using a PET/CT modality in a multicenter trial of lung cancer patients.

ACKNOWLEDGMENTS

This work was supported by the 21st Century COE program "Biomedical Imaging Technology Integration Program" funded by the Japan Society for the Promotion of Science (JSPS).

REFERENCES

1. Schrevens L, Lorent N, Dooms C, Vansteenkiste J. The role of PET scan in diagnosis, staging, and management of non-small cell lung cancer. *Oncologist.* 2004;9:633–643.
2. Higashi K, Matsunari I, Ueda Y, et al. Value of whole-body FDG PET in management of lung cancer. *Ann Nucl Med.* 2003;17:1–14.
3. Bunyaviroch T, Coleman RE. PET evaluation of lung cancer. *J Nucl Med.* 2006;47:451–469.
4. Demura Y, Tatsuro T, Ishizaki T, et al. ^{18}F-FDG accumulation with PET for differentiation between benign and malignant lesions in the thorax. *J Nucl Med.* 2003;44:540–548.
5. Gould MK, Maclean CC, Kuschner WG, Rydzak CE, Owens DK. Accuracy of positron emission tomography for diagnosis of pulmonary nodules and mass lesions: a meta-analysis. *JAMA.* 2001;285:914–924.
6. Fischer BM, Mortensen J, Hojgaard L. Positron emission tomography in the diagnosis and staging of lung cancer: a systematic, quantitative review. *Lancet Oncol.* 2001;2:659–666.
7. El-Haddad G, Zhuang H, Gupta N, Alavi A. Evolving role of positron emission tomography in the management of patients with inflammatory and other benign disorders. *Semin Nucl Med.* 2004;34:313–329.
8. Goo JM, Im JG, Do KH, et al. Pulmonary tuberculoma evaluated by means of FDG PET: findings in 10 cases. *Radiology.* 2000;216:117–121.
9. Pitman AG, Hicks RJ, Kalff V, et al. Positron emission tomography in pulmonary masses where tissue diagnosis is unhelpful or not possible. *Med J Aust.* 2001;175:303–307.
10. Sazon DA, Santiago SM, Soo Hoo GW, et al. Fluorodeoxyglucose-positron emission tomography in the detection and staging of lung cancer. *Am J Respir Crit Care Med.* 1996;153:417–421.
11. Al-Sarraf N, Gately K, Lucey J, Wilson L, McGovern E, Young V. Lymph node staging by means of positron emission tomography is less accurate in non-small cell lung cancer patients with enlarged lymph nodes: analysis of 1,145 lymph nodes. *Lung Cancer* 2008;60:62–68.
12. Shim SS, Lee KS, Kim BT, et al. Non-small cell lung cancer: prospective comparison of integrated FDG PET/CT and CT alone for preoperative staging. *Radiology.* 2005;236:1011–1019.
13. Al-Sarraf N, Aziz R, Doddakula K, et al. Factors causing inaccurate staging of mediastinal nodal involvement in non-small cell lung cancer patients staged by positron emission tomography. *Interact Cardiovasc Thorac Surg.* 2007;6:350–353.
14. Lardinois D, Weder W, Hany TF, et al. Staging of non-small-cell lung cancer with integrated positron-emission tomography and computed tomography. *N Engl J Med.* 2003;348:2500–2507.
15. Kernstine KH, Mclaughlin KA, Menda Y, et al. Can FDG-PET reduce the need for mediastinoscopy in potentially resectable nonsmall cell lung cancer? *Ann Thorac Surg.* 2002;73:394–402.
16. Poncelet AJ, Lonneux M, Coche E, et al. Groupe d'Oncologie Thoracique des Cliniques Saint-Luc. PET-FDG scan enhances but does not replace preoperative surgical staging in non-small cell lung carcinoma. *Eur J Cardiothorac Surg.* 2001;20:468–474.
17. Lowe VJ, DeLong DM, Hoffman JM, Coleman RE. Optimum scanning protocol for FDG-PET evaluation of pulmonary malignancy. *J Nucl Med.* 1995;36:883–887.
18. Hamberg LM, Hunter GJ, Alpert NM, Choi NC, Babich JW, Fischman AJ. The dose uptake ratio as an index of glucose metabolism: useful parameter or oversimplification? *J Nucl Med.* 1994;35:1308–1312.
19. Kubota K, Itoh M, Ozaki K, et al. Advantage of delayed whole-body FDG-PET imaging for tumour detection. *Eur J Nucl Med.* 2001;28:696–703.
20. Matthies A, Hickeson M, Cuchiara A, et al. Dual time point ^{18}F-FDG PET for the evaluation of pulmonary nodules. *J Nucl Med.* 2002;43:871–875.
21. Yen TC, Ng KK, Ma SY, et al. Value of dual-phase 2-fluoro-2-deoxy-d-glucose positron emission tomography in cervical cancer. *J Clin Oncol.* 2003;21:3651–3658.
22. Boerner AR, Weckesser M, Herzog H. Optimal scan time for fluorine-18 fluorodeoxyglucose positron emission tomography in breast cancer. *Eur J Nucl Med.* 1999;26:226–230.
23. Kumar R, Loving VA, Chauhan A, Zhuang H, Mitchell S, Alavi A. Potential of dual-time-point imaging to improve breast cancer diagnosis with ^{18}F-FDG PET. *J Nucl Med.* 2005;46:1819–1824.
24. Nishiyama Y, Yamamoto Y, Fukunaga K, et al. Dual-time-point ^{18}F-FDG PET for the evaluation of gallbladder carcinoma. *J Nucl Med.* 2006;47:633–638.
25. Konishi J, Yamazaki K, Tsukamoto E, et al. Mediastinal lymph node staging by FDG-PET in patients with non-small cell lung cancer: analysis of false-positive FDG-PET findings. *Respiration.* 2003;70:500–506.
26. Gould MK, Kuschner WG, Rydzak CE, et al. Test performance of positron emission tomography and computed tomography for mediastinal staging in patients with non-small-cell lung cancer: a meta-analysis. *Ann Intern Med.* 2003;139:879–892.
27. Kamel EM, Zwahlen D, Wyss MT, Stumpe KD, von Schulthess GK, Steinert HC. Whole-body ^{18}F-FDG PET improves the management of patients with small cell lung cancer. *J Nucl Med.* 2003;44:1911–1917.
28. Marom EM, McAdams HP, Erasmus JJ, et al. Staging non-small cell lung cancer with whole-body PET. *Radiology.* 1999;212:803–809.
29. Bury T, Dowlati A, Paulus P, et al. Whole-body ^{18}FDG positron emission tomography in the staging of non-small cell lung cancer. *Eur Respir J.* 1997;10:2529–2534.
30. Gupta N, Gill H, Graeber G, et al. Dynamic positron emission tomography with F-18 fluorodeoxyglucose imaging in differentiation of benign from malignant lung/mediastinal lesions. *Chest.* 1998;114:1105–1111.
31. Higashi K, Clavo AC, Wahl RL. Does FDG uptake measure proliferative activity of human cancer cells? In vitro comparison with DNA flow cytometry and tritiated thymidine uptake. *J Nucl Med.* 1993;34:414–419.
32. Duhaylongsod FG, Lowe VJ, Patz EF Jr, et al. Lung tumor growth correlates with glucose metabolism measured by fluoride-18 fluorodeoxyglucose positron emission tomography. *Ann Thorac Surg.* 1995;60:1348–1352.
33. Cook GJ, Houston S, Rubens R, Maisey MN, Fogelman I. Detection of bone metastases in breast cancer by ^{18}FDG PET: differing metabolic activity in osteoblastic and osteolytic lesions. *J Clin Oncol.* 1998;16:3375–3379.